filtration, acidification until a pH < 2 by nitric acid and storage of the samples at 4°C until analysis, there could be a loss of total arsenic content. Further, glass containers are better-suited for arsenic sampling and preservation. EDTA could be considered as an alternative preservative for the analysis of total arsenic content and its speciation. However, Bednar *et al.*[3] have prescribed varying molar concentrations of EDTA depending on Fe, Mn and other metal cation concentrations. Arsenic concentration in the unfiltered samples witnessed an increase during the first 24 h after the sampling and preservation.

Analytically, the nature of arsenic compounds present and other concomitant parameters in the contaminated samples in Kaurikasa village need a further study to explain the higher rates of arsenic loss compared to the synthetic samples or similar samples from different locations.

The results also show that the sampling and preservation artifacts may result into serious under-reporting of arsenic levels, particularly in developing countries. This is probably the major reason for the failure of scientists to reach a consensus on the dose–effect levels for arsenic. Secondly, the Indian regulators will do well if QA/QC controlled sampling and analysis is carried out for arsenic, which should encompass all the seasons in any arsenic contaminated region.

1. WHO Fact Sheet No 210, World Health Organisation, Geneva, 1999.
2. Puls, R. W. and Michael, J. B., Low-flow (minimal drawdown) ground-water sampling procedures. EPA Groundwater Issue, US EPA, 1996, vol. 540, S-95, 504.
3. Bednar, A. J., Garbarino, J. R., Ranville, J. F. and Wildeman, T. R., Preserving the distribution of inorganic arsenic species in groundwater and acid mine drainage samples. *Environ. Sci. Technol.*, 2002, **36**, 2213–2218.
4. APHA, Standards methods for the examination of water and wastewater. American Public Health Association, Washington DC, USA, 1992.
5. APHA, Standards methods for the examination of water and wastewater. American Public Health Association, Washington DC, USA, 1995.
6. US EPA, Rules and regulations. US Environmental Protection Agency), Federal Register 49, No. 209, USA, 1984.
7. WDNR, Groundwater Sampling Field Manual, Wisconsin Department of Natural Resources PUBL-DG-038 96, WDNR, USA, 1996.
8. Stolzenburg, T. R. and Nichols, D. G., Effects of filtration method and sampling devices on inorganic chemistry of sampled well water. In Proc. 6th Natl. Symp. and Exposition on Aquifer Restoration and Groundwater Monitoring, National Water Well Association, Dublin, OH, USA, 1986, pp. 216–234.
9. Pohlmann, K. F., Icopin, G. A., McArthur, R. D. and Rosal, C. G., Evaluation of sampling and field-filtration methods for the analysis of trace metals in groundwater, EPA/600/SR-94/119, 1994.
10. Pandey, P. K., Khare, R. N., Sharma, S., Sar, S. K., Pandey, M., and Binayke, P., Arsenicosis and deteriorating groundwater quality: unfolding crisis in central-east India region. *Curr. Sci.*, 1999, **77**, 686–693.
11. Pandey, P. K., Yadav, S., Nair, S. and Bhui, A., Arsenic contamination of the environment: A new perspective from central-east India. *Environ. Int.*, 2002, **28**, 235–345.
12. Acharya, S. K., Arsenic contamination in groundwater affecting major parts of southern West Bengal and parts of western Chhattisgarh: Source and mobilization process. *Curr. Sci.*, 2002, **82**, 740–744.
13. Heidlauf, D. T. and Bartlett, T. R., Effects of monitoring well purge and sample techniques on the concentration of metal analytes in unfiltered groundwater samples. Proceedings of the NGWA Outdoor Action Conference, Las Vegas, NV, USA, 1993.
14. Puls, R. W. and Barcelona, M. J., Groundwater sampling for metals analysis: EPA. Superfund Groundwater Issue, US EPA, 1989, 540, 4-89, 001, pp. 437–450.
15. HMSO, *Methods for the Examination of Waters and Associated Materials: General principles of Sampling and Accuracy of Results*, Her Majesty's Stationery Office, London England, 1980.
16. IS, *Methods of Sampling and Test (Physical and Chemical) for Water and Wastewater*, Bureau of Indian Standard, New Delhi, 1988, IS 3025, part 37.

Received 19 September 2002; revised accepted 31 December 2003

Using an optical trap to fold and align single red blood cells

J. A. Dharmadhikari and D. Mathur*

Tata Institute of Fundamental Research, 1 Homi Bhabha Road, Mumbai 400 005, India

We report on the trapping dynamics of single red blood cells (RBCs) in an optical trap. The optical trap was constructed using linearly polarized, infrared laser light (1064 nm). The trapped RBC shows folding behaviour due to the elastic nature of the cell membrane. On removal of the trap, the RBC regains its original shape, indicating that there is no cell damage induced by the optical field. The folding time for the RBC is less than 1 s, while the relaxation time is ~ 6 s. The folded RBC aligns itself along the direction of the electric field of the laser due to the action of polarization-induced forces; introducing a half-wave plate in the trap and forcing the trapped RBC to follow the direction of the electric field vector of the laser confirms this.

THE utility of optical tweezers to trap and manipulate microparticles is now well established[1]. In recent years, the advent of optical tweezers has opened new vistas for both basic and applied research in diverse areas of life sciences, like single-cell molecular biology[2], laser-assisted *in vitro* fertilization[3], development of cell biosensors[4], micromanipulation of relevance to cell sorting and cellular microchips[4,5] and studies of the mechanics of single DNA molecules[6]. Optical trapping also makes feasible single-cell testing of erythrocytes that are linked to pharmacophores for use in drug therapy[7].

*For correspondence. (e-mail: atmol1@tifr.res.in)

In a typical optical tweezers set-up, the action of a strongly focused laser beam on a dielectric material gives rise to two types of forces. The strong focusing of the laser light generates a gradient force, F_g, which exerts a pull on dielectric particles towards the focal zone. On the other hand, there are scattering forces, F_s, which push the particles away from the focus, towards the incident light direction. The magnitude of the total force that is generated in optical traps is $F = (F_s^2 + F_g^2)^{1/2}$. When the magnitude of F_g is greater than F_s, optical trapping occurs. For laser power P, typically ca. 30 mW at the location of the trapped material, the momentum of the light beam that is experienced per second, $F \sim Pn/c$ (where n is the refractive index of the solvent in which the dielectric microparticles are made to float, and c is the speed of light in vacuum), is in the range of pico-Newton (PN).

The primary function of optical tweezers has, in the main, been to fix and manipulate the position of a microparticle within the focal volume of the laser. In many cases the orientation of the trapped particle has been considered to be irrelevant. Indeed, in the case of bodies with spherical symmetry, the nature of the light-induced forces is such that it is impossible to influence the orientation. However, it is clear that exercise of control over all motional degrees of freedom of trapped particles would add an extra dimension to the capabilities of optical traps, and would constitute a distinct added advantage in many spheres of contemporary research activity that utilize optical tweezers.

We have designed and built an optical trap so as to explore the possibilities of exercising motional control on trapped dielectric particles. We report here on the trapping dynamics of the red blood cells (RBCs) in an optical trap that is formed by a linearly polarized, TEM_{00} mode, infrared laser beam. The normal shape of a human RBC is a flattened biconcave disk whose diameter is about 7 μm, and whose thickness varies from about 0.9 μm at the thinnest central portion of the disk to 2.1 μm at the largest part near the periphery[8]. Due to the elastic nature of the cell membrane in an RBC, we considered it likely that upon its placement in an optical trap, the trapped RBC may deform its shape and this, indeed, turns out to be the case. Moreover, we have discovered that trapped RBCs not only change their morphology, but they also tend to align such that the symmetry axis of the cell aligns along the direction of the laser polarization vector. The original shape of the RBC, as well as its initial random orientation is regained once the optical trap is switched-off.

There has been one previous report on trapping of RBCs with single-beam optical trap, but one that uses a complicated higher order TEM_{0n} laser beam[9]. A dual-beam trap has also been used for trapping RBCs by attaching beads to both ends of the cell and trapping each of the beads to study the elastic stretching behaviour[10]. As of today, and to the best of our knowledge, there are no reports published on the behaviour of RBCs when trapped with a single-beam optical trap that is formed by a TEM_{00} laser beam. However, optical trapping of long, artificially fabricated cylinders with their symmetry axes along the laser beam has been predicted[11] and observed[12]. Light scattered by trapped microspheres has also been studied[13,14]. The paucity of information does not detract from the fact that interaction between light and asymmetric dielectric particles is important, as many naturally occurring particles that have the potential to be tweezed are not spherical.

The trapping of RBCs in our experiments was carried out using a single-beam optical trap. The trapping dynamics was recorded in real time with the CCD camera attached to an inverted microscope. The salient features of our optical trap are presented in the following.

Figure 1 presents a schematic depiction of our optical tweezer set-up which essentially comprised an infrared laser radiating in the infrared at a wavelength of 1064 nm, and an inverted optical microscope that were mounted on a pressurized vibration isolation table in order to minimize noise due to vibrations. An essential feature of the apparatus was an oil immersion, large numerical aperture (NA = 1.3) 100X objective that was utilized to strongly focus the laser beam onto the target cells placed on an ordinary glass microscopy slide. Our microscope objective had a transmission of 65% at 1064 nm light. The infrared light was obtained from a solid-state, diode pumped $Nd:YVO_4$ laser. The results that we report in the follow-

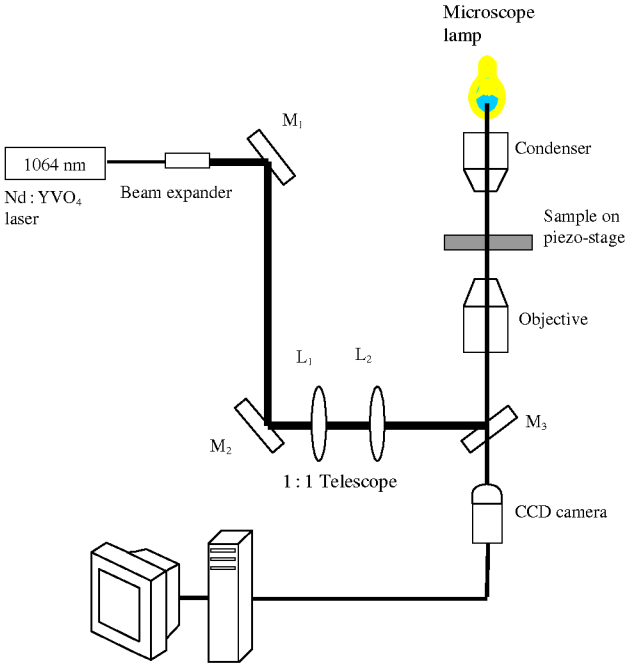

Figure 1. Schematic of optical tweezer set-up. All components shown, including the vibration isolation table, are procured locally except for the inverted microscope (Nikon, Japan) and the nanometer resolution piezoelectric stage (Piezosystem, Jena, Germany). The authors can be contacted for further information.

ing were obtained using an incident laser power of 100 mW, although after transmission through the oil-filled objective, typical powers incident on the microscope slide were ~30 mW. The wavelength of 1064 nm was chosen so as to minimize heating of the sample and, perhaps more importantly, to avoid photo-damage. We note that most biological samples have negligible absorption in the near infrared part of the electromagnetic spectrum[15].

The back focal plane of the objective lens had a diameter of nearly 6 mm, whereas the diameter of the incident laser beam was around 0.9 mm. The beam diameter of the laser was measured using knife-edge method. In order to obtain a near-diffraction-limited spot size when the laser light is tightly focused, it is necessary to ensure that the back focal plane of the objective is overfilled. In order to achieve this, the infrared beam was expanded using an optical-beam expander that was anti-reflection-coated for 1064 nm wavelength. A typical beam diameter of 7 mm was obtained from our beam expander. The focused spot size also depends on the quality of the laser beam, specifically on the number of electromagnetic modes that are present in the beam. In our case beam quality of the laser was found to be good, with a perfect TEM_{00} mode. Figure 2 depicts a typical beam profile that we measured using a photodiode mounted behind a moving small aperture comprising horizontal and vertical razor blades mounted on a translation stage that scanned across the laser beam. Quantification of the laser-beam quality can be made in terms of a quality factor, M^2, which is defined as the ratio of the product of the waist diameter and angular divergence of our laser to the waist diameter–divergence product of a theoretical Gaussian profile. For an ideal laser output that is Gaussian in shape, it is clear that $M^2 = 1$; for a practical laser beam, it is expected that $M^2 > 1$, with the closeness to unity defining the 'goodness' of beam quality. We measured the value of M^2 for our laser beam to be 1.19, indicating a beam quality that can be considered very good by present standards.

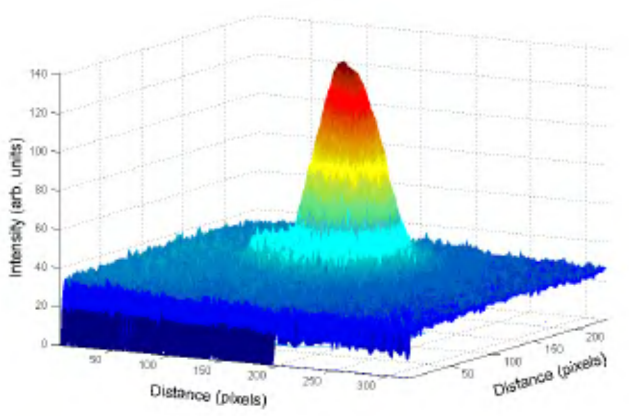

Figure 2. Three-dimensional beam profile of the unfocused laser beam. Distance scale represents the actual number of pixels illuminated on the CCD camera (see text).

Manual steering of the laser beam was achieved using a set of two convex lenses, L_1 and L_2, with equal focal length. The two lenses are kept at a distance of $2f$ (f is the focal length) from each other as well as from the back focal plane of the objective. A mirror that was highly reflecting at 1064 nm wavelength, M_3, was kept at an angle of 45° and was used to reflect the laser beam into the microscope objective. The mirror would, thus, reflect the 1064 nm wavelength and transmit all the other radiations, enabling us to accomplish imaging simultaneously with trapping.

A piezoelectric stage with a total travel length of 100 μm, and with a spatial resolution of 100 nm, was used in the set-up to achieve precise nanometer displacements of the sample. The piezoelectric stage could be operated in two different modes: (i) a manual mode in which the stage could be moved manually by changing the voltage applied to the piezo crystal, and (ii) by applying a modulated input signal, typically varying from 0 to 10 V, to control the position of the stage. In our case, we generated the 0–10 V modulated signal using a computer-data-acquisition card that was interfaced to the position controller through a shielded BNC cable and connector board.

A major advantage of using an inverted microscope in an optical trap such as ours is that the same objective that is used to strongly focus the light onto the sample also acts as a condenser to collect light that is reflected from the sample. As already noted, this reflected light is transmitted by the mirror M_3, and is then collected onto a CCD camera that is mounted on one of the ports of the microscope. An infrared filter was placed in front of the CCD camera to prevent damage by the laser beam. The CCD camera, along with the TV card, was connected to a computer to record real time images of the sample within the trap. The pixel size in our CCD camera was 9 μm and a frame-grabbing speed of 25 frames s^{-1} was used in our experiments. With our camera speed the temporal resolution of the measurements we report here was 40 ms.

A number of methods can be employed to determine the strength of an optical trap such as ours. The most common and perhaps the simplest method is the so-called escape force method[16]; we adopted this method for our present experiments. Simply put, this method relies on determination of the minimal force that is required to pull an object out of the trap. One simple way of generating external forces of variable strength for this purpose is by imposing a viscous drag force on the trapped microparticle; the magnitude of such forces can be readily computed using classical mechanics[17,18]. To produce the necessary drag force, the particle may either be pulled through a fluid (by moving the optical trap relative to a stationary translation stage), or more conventionally, the fluid itself can be moved past the particle (by moving the translation stage relative to a stationary trap).

A number of variants of the viscous drag method are possible as far as practical implementation is concerned.

One of the simplest is to videotape a trapped particle in a fixed trap while translating the microscope stage (e.g. by hand) at an ever-increasing rate, until the particle just escapes. The particle escape velocity is measured from the video record, which enables estimation of the escape force, provided the viscous drag coefficient of the particle is known. This technique permits calibration of force to an accuracy of within about 10%. If, instead, the stage is moved at a fixed, known velocity, the laser trapping power can be reduced until the particle just escapes; this method provides somewhat better reproducibility of measurements. Note that escape forces are determined by optical properties at the very edges of the trap, where the restoring force is no longer a linear function of the displacement[19]. Since the measurement is not at the centre of the trap, the trap stiffness cannot be ascertained. Escape forces are generally somewhat different in the x, y and z directions, so the exact escape path must be determined for precise measurements.

In our measurements, the laser power was found to be ~20 mW at the sample. We calibrated the strength of our tweezer set-up by optically trapping polystyrene beads of 5 μm diameter. The viscous force measured in our optical trap was ~ 12 pN.

Typical behaviour of normal RBCs in our optical trap is depicted in Figure 3. The different panels (*a–d*) depict the real-time folding of a single trapped RBC: within a time period of 760 ms after initial exposure to the trapping laser beam, the flat biconcave disk shape of a normal RBC is altered into a folded pattern. Such folding is not inconsistent with the known morphology of these cells. The ratio of volume to surface area for RBCs is smaller than that for spherical objects of the same size. For identical surface areas, the ratio of the RBC volume to spherical volume is significantly less than unity[20], ~ 0.6. It is, therefore, not unreasonable to expect that energy constraints will not seriously impede RBCs from readily assuming different non-spherical shapes.

The elastic response of an RBC to an applied force of the type that is exerted by the focused laser beam, is likely to be determined essentially by the cell membrane as the inner fluid has no elasticity by virtue of it being purely viscous. In terms of two-dimensional laws of elasticity[21], the elastic shear modulus, μ, of the cell membrane and the area compressibility, K, determine the dynamics that is responsible for the observed morphological changes in the RBCs. The elastic properties of the cytoskeleton determine the magnitude of μ, while K is controlled by the almost incompressible phospholipidic bilayer. For RBCs, it is established[22] that $K \gg \mu$. Thus, the folding and unfolding that are observed proceed in such manner that the elastic properties of the cytoskeleton come into play, while the overall area of the cytoskeleton remains constant. From a biological point of view, this facet of RBC behaviour is important as such cells need to pass through blood vessels that have variable diameter. The structure of the RBC is such that it can penetrate even through the narrow-diameter vessels by appropriate morphological

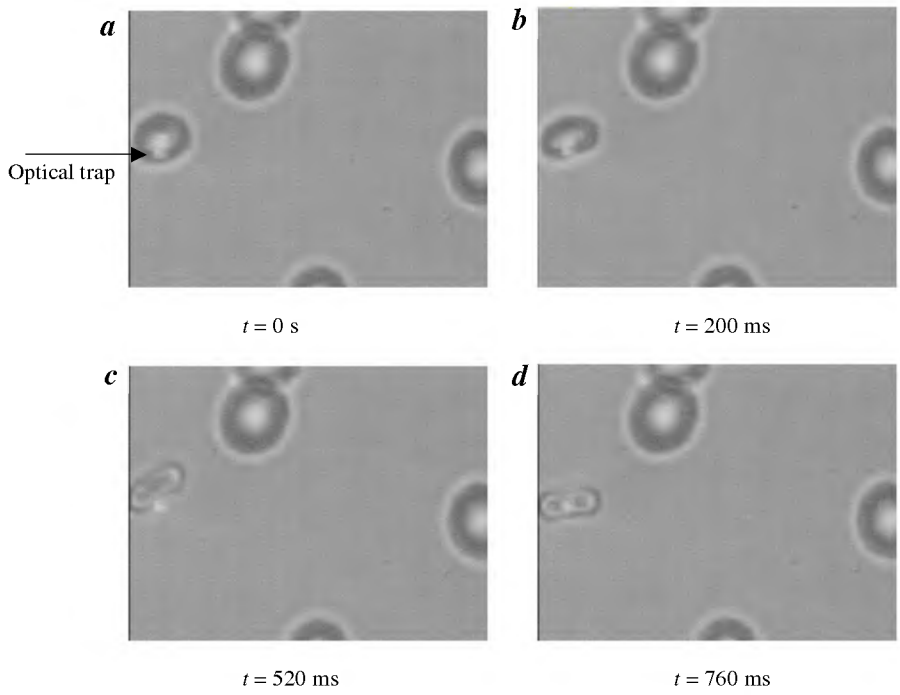

Figure 3. Real-time folding sequence of an RBC [(*a*) through (*d*), covering the time range up to 760 ms)].

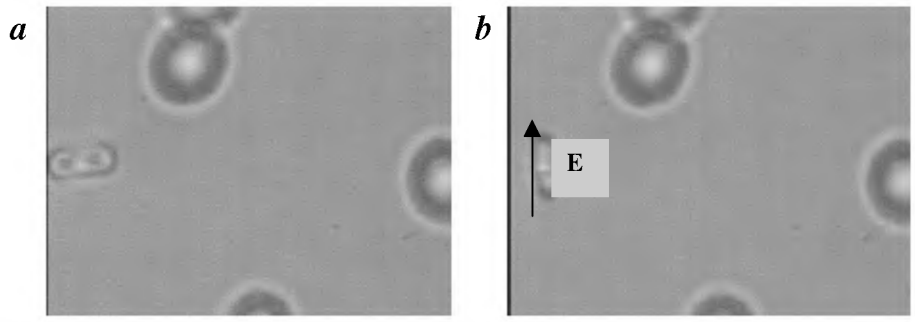

Figure 4. Alignment of folded RBC along the electric field vector (denoted as **E**). At $t = 0$ s, the RBC is completely folded within the trap (***a***). After another second, the RBC aligns itself along the electric field vector (***b***); arrow points in the direction of the electric field of the laser.

changes. The elasticity in such cases, including the folding that we depict in Figure 3, is expected to be due to the cell membrane.

Figure 4 shows that once the RBC has folded, the interaction with the focused laser beam does not end. There is a change in the direction of the folded RBC, such that the major symmetry axis lines up in a direction that is parallel to the direction of the laser polarization vector (indicated by an arrow in the figure). Taking an RBC to be a non-absorbing, asymmetric, dielectric object, the linearly polarized light beam used to make our optical trap possesses an electric field, **E**, whose direction is well defined, and can be readily varied by means of a $\lambda/2$ plate that is placed in the path of the laser beam. This field induces a dipole moment $\mathbf{p} = \acute{\alpha}.\mathbf{E}$, where $\acute{\alpha}$ is the polarizability tensor of the RBC whose intrinsic asymmetry implies that polarizability components parallel and perpendicular to the RBC axis ($\alpha_{\parallel}$ and $\alpha_{\perp}$, respectively) are significantly different from each other. If one draws the analogy between a folded RBC and a rigid rotor interacting with a uniform electric field **E**, the interaction potential that governs the dynamics of laser–RBC interaction can be expressed as

$$V_{\alpha} = \frac{-E^2}{2}(\alpha_{\text{parallel}} \cos^2\theta + \alpha_{\text{perpendicular}} \sin^2\theta),$$

where θ denotes the angle between the major symmetry axis of the RBC and the **E**-vector. In terms that are used by molecular spectroscopists, the situation that results from both components, $\alpha_{\parallel}$ and $\alpha_{\perp}$, being equal is that of a free rigid rotor. In our case, it is the difference in magnitude of $\alpha_{\parallel}$ and $\alpha_{\perp}$ that gives rise to spatial alignment of the folded RBC.

This difference in polarizability components comes into play in the form of the resulting light-induced torque that is generated, $\hat{\mathbf{o}} = \mathbf{p} \times \mathbf{E}$, such that energy minimization constraints induce in the trapped RBC a 'kick' in a direction that leads to alignment along the direction of the **E**-field vector. We have made measurements to confirm the alignment of the RBCs along the **E**-vector by putting a half-wave plate that enables us to alter the direction of the **E**-vector. The trapped and folded RBC faithfully followed the direction of the **E**-vector in our experiments. The unfolding behaviour of the RBC shows that there is no apparent damage to the RBC due the laser radiation.

It is important to reiterate here that our experiments have been conducted using linearly polarized light from a TEM_{00} mode laser. Light-induced motion of absorbing microscopic particles has, indeed, been demonstrated in earlier experiments, but only in ones that were more complex in that they either utilized elliptically polarized light[23], or used laser beams with helical phase structure[24]. Earlier work using linearly polarized laser light has trapped only artificially-fabricated birefringent microparticles, such as optical disks made of wax and polymethylmethacrylate that have recently been trapped, such that the trapped disks align themselves so as to achieve edge-on orientation with respect to the incident laser-beam direction[24].

We have designed and built an optical tweezer set-up using an infrared laser operating at 1064 nm wavelength. The trap has strength of the order of a few tens of pN, with sub-pN sensitivity. The piezo-stage is used that yields nanometre-scale precision. Human RBCs were trapped using linearly polarized light. Due to the elastic nature of the RBC, folding behaviour is observed upon trapping. When the trap is removed, the RBC regains its original shape. The folding time is measured to be of the order of 760 ms, while relaxation to the original biconcave disk shape takes much longer (about 6 s). The trapped, folded RBC aligns itself along the direction of electric field vector of the laser; this was confirmed by making measurements with a $\lambda/2$ plate that enables us to orient the trapped, folded RBC in a direction that is determined by the half-wave plate. The type of dynamics that we have observed is of importance from the viewpoint of developing cellular motors, and further work in this direction is proceeding in our laboratory.

A report on how infection of an RBC by the malarial parasite, *Plasmodium falciparum* affects the optical trapping characteristics and induces extraordinarily large torques that result in rotational motion of the trapped, infected cell has been published recently[25].

1. Ashkin, A., Dziedzic, J. M., Bjorkholm, J. E. and Chu, S., Observation of a single-beam gradient force optical trap for dielectric particles. *Opt. Lett.*, 1986, **11**, 288–290.
2. Schutze, K., Posl, G. and Lahr, G., Laser micromanipulation systems as universal tools in cellular and molecular biology and in medicine. *Cell. Mol. Biol.*, 1998, **44**, 735–746.
3. Zahn, M. and Seeger, S., Optical tweezers in pharmacology. *Cell. Mol. Biol.*, 1998, **44**, 747–761.
4. Clement-Sengewald, A., Schutze, K., Ashkin, A., Palma, G. A., Kerlen, G. and Brem, G., Fertilization of bovine oocytesinduced solely with combined laser microbeam and optical tweezers. *J. Assisted Reprod. Genet.*, 1996, **13**, 259–265.
5. Zahn, M., Renken, J. and Seeger, S., Fluorimetric multiparameter cell assay at the single cell level fabricated by optical tweezers. *FEBS Lett.*, 1999, **443**, 337–340.
6. Bustamante, C., Bryant, Z. and Smith, S. B., Ten years of tension: single-molecule DNA mechanics. *Nature*, 2003, **421**, 423–427.
7. Krantz, A., Red-cell mediated therapy: opportunities and challenges. *Blood Cells, Mol. Dis.*, 1997, **23**, 58–68.
8. Sato, S., Ishigure, M. and Inaba, H., Optical trapping and rotational manipulation of microscopic particles and biological cells using higher-order mode Nd-YAG laser beams. *Electr. Lett.*, 1991, **27**, 1831–1832.
9. Guck, J., Ananthakrishnan, R., Mahmood, H., Moon, T. J., Cunningham, C. C. and Kas, J., The optical stretcher: A novel laser tool to micromanipulate cells. *Biophys. J.*, 2001, **81**, 767–784.
10. Gaithier. R. C., Theoretical investigation of the optical trapping force and torque on cylindrical micro-objects. *J. Opt. Soc. Am. B*, 1997, **14**, 3323–3333.
11. Gaithier, R. C., Ashman, M. and Grover, C. P., Experimental confirmation of the optical-trapping properties of cylindrical objects. *Appl. Opt.*, 1999, **38**, 4861–4869.
12. Bar-Ziv, R., Meller, A., Tlusty, T., Moses, E., Stavans, J. and Safran, S. A., Localized dynamic light scattering: Probing single particle dynamics at the nanoscale. *Phys. Rev. Lett.*, 1997, **78**, 154–157.
13. Meller, A., Bar-Ziv, R., Tlusty, T., Moses, E., Stavans, J. and Safran, S. A., Localized dynamic light scattering: A new approach to dynamic measurements in optical microscopy. *Biophys. J.*, 1998, **74**, 1541–1548.
14. Elgsaeter, A., Stokke, B. T., Mikkelsedn, A. and Branton, D., The molecular basis of erythrocytes shape. *Science*, 1986, **234**, 1217–1223.
15. Neuman, K. C., Chadd, E. H., Liou, G. F., Bergman, K. and Block, S. M., Characterization of photodamage to *Escherichia coli* in optical traps. *Biophys. J.*, 1999, **77**, 2856–2863.
16. Ashkin, A., Schuetze, K., Dziedzic, J. M., Euteneuer, U. and Schliwa, M., Force generation of organelle transport measured *in vivo* by an infrared laser trap. *Nature*, 1990, **348**, 346–348.
17. Block, S. M., Blair, D. F. and Berg, H. C., Compliance of bacterial flagella measured with optical tweezers. *Nature*, 1989, **338**, 514–518.
18. Svoboda, K. and Block, S. M., Biological applications of optical forces. *Annu. Rev. Biophys. Biomol. Struct.*, 1994, **23**, 247–285.
19. Mukhopadhyay, R., Lim, G. H. W. and Wortis, M., Echinocyte shapes: bending, stretching, and shear determine spicule shape and spacing. *Biophys. J.*, 2002, **82**, 1756–1772.
20. Landau, L. D. and Lifshitz, E. M., *Theory of Elasticity*, Pergamon Press, New York, 1959, p. 56.
21. Henon, S., Lenormand, G., Richert, A. and Gallet, F., A new determination of the shear modulus of the human erythrocyte membrane using optical tweezers. *Biophys. J.*, 1999, **76**, 1145–1151.
22. Friese, M. E. J., Enger, J, Rubinsztein-Dunlop, H. and Heckenberg, R. N., Optical angular-momentum transfer to trapped absorbing particles. *Phys. Rev. A*, 1996, **54**, 1593–1596.
23. Simpson, N. B., Dholakia, K., Allen, N. and Padgett, M. J., Mechanical equivalent of the spin and orbital angular momentum of light: an optical spanner. *Opt. Lett.*, 1997, **22**, 52–54.
24. Cheng, Z., Chaikin, P. M. and Mason, T. G., Light streak tracking of optically trapped thin microdisks. *Phys. Rev. Lett.*, 2002, **89**, 108303 1–4.
25. Dharmadhikari, J. A., Roy, S., Dharmadhikari, A. K., Sharma, S., and Mathur, D., Torque-generating malaria-infected red blood cells. *Opt. Express*, 2004, **12**, 1179–1184.

ACKNOWLEDGEMENTS. We have benefited from many stimulating discussions with our colleagues, B. J. Rao and Sunil Noothi, which have helped us design and fabricate the optical trap to study the manipulation of single biomolecules. We are grateful to Shobhona Sharma and Sunando Roy for providing red blood cell samples used in these experiments. Useful discussions with them and with R. G. Pillay, M. Krishnamurthy and Amit Roy are acknowledged. We thank Sakti Narayan for initial measurements of some of the laser parameters.

Received 3 January 2004; accepted 7 April 2004

A combined approach of Schlumberger and axial pole–dipole configurations for groundwater exploration in hard-rock areas

S. Chandra*, V. Anand Rao and V. S. Singh

Groundwater Exploration and Management Group, National Geophysical Research Institute, Uppal Road, Hyderabad 500 007, India

In hard rocks, groundwater accumulation occurs only because of secondary porosity developed due to weathering, fracturing, faulting, etc., which is highly variable and varies sharply within very short distances, contributing to near-surface inhomogeneity. This can affect the current-flow pattern in their surroundings and consequently distort the resistivity curve, and hence falsify the interpretation in terms of layer resistivity and its thickness. Thus it becomes a difficult task for locating a good well site in hard rocks. A combined approach of Schlumberger and axial pole–dipole configurations has been initiated, which will be helpful in locating the successful sites for drilling of wells in hard-rock areas. It is also suggested that the axial pole–dipole array can be applied for groundwater exploration even at places where Schlumberger

*For correspondence. (e-mail: chandra_sngri@rediffmail.com)